Anderson localization induced by gauge-invariant bond-sign disorder in square PbSe nanocrystal lattices

Athmane Tadjine and Christophe Delerue*
[1]*Univ. Lille, CNRS, Centrale Lille, ISEN, Univ. Valenciennes, UMR 8520 - IEMN, F-59000 Lille, France*

(Received 22 February 2018; revised manuscript received 13 July 2018; published 17 September 2018)

We study theoretically the problem of electrons moving on a two-dimensional square lattice characterized by nearest-neighbor hopping terms of constant amplitude but random sign. The original motivation came from the discovery that this "bond-sign" disorder can be present in square lattices of epitaxially connected PbSe nanocrystals, which have been recently synthesized using colloidal routes. We investigate how this type of disorder tends to localize the electronic wave-functions and modifies the electronic structure. This is done via the calculation of the density-of-states, the participation ratio and the localization length. We show that, when the relative fraction p of negative signs increases from 0% to 50%, the effect of the disorder on the wave functions saturates at a constant level when p reaches values above ∼25%. This behavior reveals that the true disorder experienced by the electrons is not the nominal disorder defined by p but a smaller part of it, which is irreducible due to frustrations. The amount of true disorder can be obtained by successive local gauge transformations as developed in the past to study models of spin glasses. In the thermodynamic limit, this irreducible gauge-invariant disorder induces localization of all electronic states, except at the center of the band where our calculations suggest that zero-energy states have a critical behavior. The particle-hole symmetry, which characterizes these disordered systems plays a crucial role in this behavior, as already found in lattices with random hopping or random magnetic flux, for example. In the case of lattices of PbSe nanocrystals, the effects of the bond-sign disorder are found to be weaker than those of more conventional types of disorder.

DOI: 10.1103/PhysRevB.98.125412

I. INTRODUCTION

The localization of waves propagating in disordered media remains one of the most universal problem in physics. Sixty years after the seminal work of Anderson [1], it is now well-known that localization properties depend not only on the dimensionality of the media [1–3] but also on their fundamental symmetries (time-reversal, spin-rotation, chirality, parity). On the theoretical side, Anderson localization was mostly investigated for electrons on lattices with a single orbital per site. The disorder is usually introduced in the tight-binding Hamiltonian as a random distribution of the onsite energy E_0 [1,3] or the nearest-neighbor hopping term t [4–8], or by a fraction of missing bonds [9–11]. The predictions of these models were verified experimentally with photons [12–14] acoustic waves [15,16], and matter waves [17,18]. These theoretical models are also very useful to study the effect of the disorder on the electronic and transport properties of semiconductor nanocrystal (NC) assemblies [19–24].

In this paper, we investigate a type of disorder (hereafter, bond-sign disorder), which has received little attention up to now [25], even if we will see that it presents important similarities with classes of disorder models that received considerable attention in particular for the investigation of critical points and wave functions [26–36]. Our initial motivation came from the recent synthesis of novel 2D materials using PbSe colloidal NCs as building blocks (more generally PbX NCs, X = Se, S, Te) [37–39]. The PbSe NCs, characterized by a truncated cubic shape, spontaneously self-assemble into a long-range ordered square (super)lattices by forming epitaxial connections via the {100} facets of the nanocubes [Fig. 1(a)]. Before formation of the lattice, each individual NC approximately behaves as a spherical quantum dot. Its highest hole (valence) and lowest electron (conduction) states can be seen as standing waves characterized by a S-like envelope wave function. In the 2D lattices, the electronic coupling between neighbor NCs leads to the formation of energy bands which can be well described by an effective Hamiltonian in which each site represents a NC, E_0 is the S-state energy, and t accounts for the coupling between the S states of nearest-neighbor NCs [40,41]. In a 2D square lattice of parameter a (typically of the order of 5 nm), this leads to a band dispersion of the form

$$E(\mathbf{k}) = E_0 + 2t[\cos(k_x a) + \cos(k_y a)], \tag{1}$$

where $\mathbf{k} = (k_x, k_y)$ is the 2D wave vector (see examples in Fig. 2).

This effective model was recently used to study the effects of the disorder (NC polydispersity, fraction of missing bonds) on the transport properties in these lattices of epitaxially-connected NCs [22,42]. In the most logical way, the disorder was characterized by distributions of E_0 and t, and by a certain percentage of broken bonds ($t = 0$). However, there are additional nonconventional sources of disorder which were not considered (however, see Supplementary Information of Ref. [42]). Indeed, in each NC, the true wave functions

*christophe.delerue@iemn.univ-lille1.fr

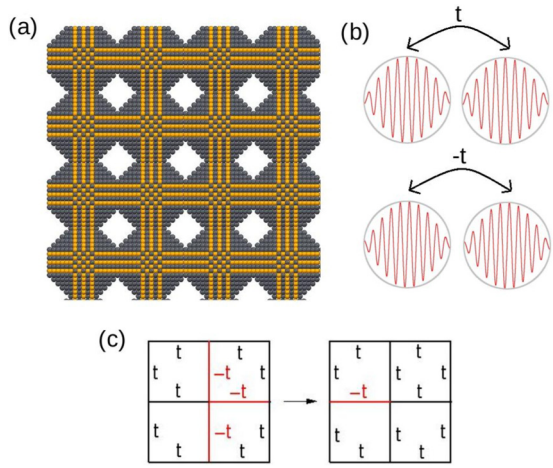

FIG. 1. (a) Top view of a square lattice of PbSe NCs attached via {100} facets. Each NC has a truncated nanocube shape with six {100}, eight {111}, and twelve {110} facets. Grey/dark colored (gold/light colored) spheres are used to indicate Pb (Se) atoms, respectively. (b) Schematic view of the electron wave function in two neighbor NCs, showing two situations with hopping terms (t) of opposite sign. (c) Selected section of a square lattice with bonds characterized by a hopping term t or $-t$. The unitary transformation consisting in changing the sign of the orbital at the center of the section allows to reduce the number of bonds with negative sign.

are not just S-like orbitals but are actually the product of the S-like envelope by the Bloch wave function at the bulk semiconductor band edge [43]. In the case of PX materials, the valence and conduction band extrema are at the L point of the Brillouin zone and are fourfold degenerate [44].

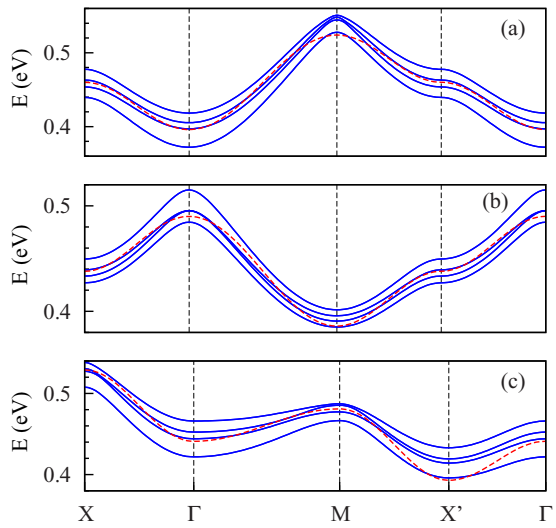

FIG. 2. (a) Lowest conduction bands (blue solid lines) calculated for a square lattice of PbSe NCs. The distance between centers of nearest-neighbor NCs, i.e., the lattice parameter, is given by $a = na_0$, where $n = 8$. The red solid line presents the energy dispersion given by Eq. (1) with $E_0 = 0.460$ eV and $t = -0.032$ eV. (b) Same but for $n = 9$, $E_0 = 0.438$ eV, and $t = +0.026$ eV. (c) Same but for a rectangular lattice characterized by $E_0 = 0.461$ eV, $n = 8$ along the [100] direction ($t = -0.044$ eV), and by $n = 9$ along [010] ($t = +0.024$ eV).

Therefore, in each PbX NC, the lowest conduction (highest valence) states are composed of a manifold of eight states (including spin degeneracy). The degeneracy of these states is slightly lifted due to inter-valley couplings induced by the quantum confinement [44]. When identical NCs are attached to form a 2D square lattice, this leads to the formation of four (twofold degenerate) bands instead of one, but their energy dispersion is still approximately described by Eq. (1), as shown in Figs. 2(a) and 2(b) presenting two typical conduction band structures calculated using the methodology described in Appendix A.

However, the comparison between Figs. 2(a) and 2(b) reveals a remarkable feature: the two band structures are characterized by couplings t of opposite sign. These band structures are calculated for square lattices of PbSe NCs characterized by a (super)lattice parameter $a = na_0$ (distance between NC centers), where a_0 is the (microscopic) lattice parameter of bulk PbSe and n is an integer, as required by the periodicity of the superlattice [Fig. 1(a)]. Figures 2(a) and 2(b) are obtained for $n = 8$ and 9, respectively. In fact, it was shown in Ref. [40] that the sign of t depends on the parity of n. This sign is determined by the rapidly oscillating Bloch-function part of the electron (hole) wave function in each NC, as schematically depicted in Fig. 1(b). As a matter of fact, Fig. 2(c) shows that, for a rectangular lattice defined by $n = 8$ and 9 in the [100] and [010] directions, respectively, the energy dispersion is characterized by hopping terms of opposite sign along the two directions.

In this context, the NC size dispersion naturally present in lattices of PbX NCs should result in bond-sign disorder, in addition to other types of disorder [42]. It is not possible to incorporate these effects into atomistic tight-binding calculations due to computational limits. Therefore, in the following, we use the effective lattice Hamiltonian model to study the effect of the bond-sign disorder alone in order to identify its specific properties. We will see that, among other results, this study establishes unexpected links between different areas of condensed matter physics, from colloidal NCs to spin glasses, from the band structure of superlattices to the concepts of gauge invariance and frustrations [25,45–47].

In this work, our main goal is to investigate the general effects of bond-sign disorder on the quantum states of electrons on square lattices in order to predict their influence in particular in the case of lattices of PbSe NCs. We consider systems in which the hopping term can take only two opposite values, $\pm t$, with a probability p for $-t$ (by convention, $E_0 = 0$, $t > 0$). We show that p, which characterizes the nominal disorder, does not represent its real effect on the electronic states. In close analogy with the theoretical treatments on the Ising model of spin glass [25], the amount of apparent disorder can be reduced by successive gauge transformations. In 1D lattices, this reduction is total in such a way that there is no real disorder, whatever p [48]. In contrast, in 2D square lattices, Anderson localization takes place due to the existence of a gauge-invariant (GI) disorder (or frustration [45]) actually seen by the electrons. We characterize this true (real) disorder by p_r, the minimum fraction of bonds with negative sign obtained by gauge transformations (other measures of the disorder are possible). This GI disorder p_r almost coincides with the nominal disorder for p below $\sim$10%. When p is

further increased, the amount of real disorder varies sublinearly and finally saturates at a constant value for $25\% \lesssim p < 50\%$ [49]. In this work, we calculate the participation ratio, which measures the localization of the electronic states, and the fourth moment of the density of states (DOS). These two quantities allow to characterize the effects of the GI disorder and their variations with the nominal disorder. We quantify the localization effect of the GI disorder by calculating the localization length versus electron energy. We conclude that, in lattices of PbSe NCs, the bond-sign disorder has relatively weak influence compared to more conventional disorders [42]. We also show that zero-energy states are delocalized in contrast to the others, for reasons, which were already identified in disordered lattices presenting a similar chiral symmetry [26–36],

The results presented here are totally universal since they do not depend on the value of $|t|$. Therefore the control of the sign of the effective hopping term in systems other than NC lattices should be of high fundamental interest in order to study the effect of bond-sign disorder. The scientific context for such studies is favorable since many experiments recently concerned the investigation of optical, acoustic, and matter waves in artificial lattices [13,16–18,50–52].

II. GAUGE-INVARIANT DISORDER

A. Gauge transformation

We consider a square lattice of $N \times N$ sites, with a one S orbital per site. For convenience, we assume periodic boundary conditions. Without loss of generality, the nearest-neighbor hopping term is set to $|t| = 1$ and the on-site energy of each orbital $E_s = 0$. The Hamiltonian matrix elements can be written as [25]

$$H_{ij} = \pm 1, \text{ if } i \ @ \ j = 0 \text{ otherwise}, \tag{2}$$

where @ refers to adjacent sites. H is thus a symmetric matrix of dimension N^2.

We start with a nominal disorder defined by p. In most cases, the number of "negative bonds" can be reduced by successive unitary transformations, without changing the nature of the system [25,48]. Each operation is a local gauge transformation consisting in changing one orbital of the tight-binding basis into its opposite, which reverts the sign of all bonds connected to this site [Fig. 1(c)]. By definition, if we consider all possible transformations, we can find a configuration with a minimum number of negative bonds that defines the GI disorder (see below for details). We will see that the GI disorder is the true one probed by the electrons.

1. Equivalent representations and irreducible configurations

Important properties arise from the definition of Eq. (2). H has 2^{N^2-1} representations that keep the determinant unchanged. These representations correspond to multiplying the atomic orbitals by a minus sign. These 2^{N^2-1} permutations constitute a class of equivalent elements. It is important to note that if there are more than 2^{N^2-1} possible configurations for the lattice, then there must be several classes.

Under periodic boundary conditions, each site has V bonds. The number of total bonds in the system are given by $N_b = \frac{N^2 V}{2}$. The factor $\frac{1}{2}$ prevents from counting the same bond twice. The configuration space, determined by all possible generated Hamiltonians, contains $N_{Cf} = 2^{N_b} = 2^{\frac{N^2 V}{2}}$ elements, since each bond can take two values (± 1) independently from the values of the other bonds. Using the property that each of these elements has 2^{N^2-1} equivalent representations, we obtain the number of equivalence classes $N_{Cl} = \frac{2^{\frac{N^2 V}{2}}}{2^{N^2-1}} = 2^{N^2(\frac{V}{2}-1)+1}$.

At this point, we define an irreducible configuration as a configuration in which the number of negative bonds cannot be lowered by any series of permutations. This implies by definition that each class has at least one irreducible configuration which corresponds to the one with the lowest number of negative bonds.

2. 1D Case

In 1D lattices with periodic boundary conditions ($V = 2$), the number of classes N_{Cl} is 2. It can be easily demonstrated that any nominal disorder can be reduced to a configuration with either zero or one irreducible negative bond in the chain [48]. Therefore all 1D lattices behave as perfectly ordered chains (no GI disorder), all states are delocalized whatever p.

3. 2D case

For $V > 2$, which is the case of 2D lattices, the number of classes scales with N. Also, the number of classes is always $\geqslant 2$, meaning that there are always configurations with negative bonds that cannot be reduced to zero negative ones.

In contrast with the 1D case, the classes are no longer defined by the number of irreducible negative bonds. Two irreducible configurations with a given number of negative bonds do not necessarily belong to the same class. As an example, we take the simple case of one negative bond on the ith atom. The atom has four total bonds, hence there are four possible configurations of choosing one of them to be negative. All of these four configurations cannot belong to the same class because there is no way of changing the position of the negative bond around the ith atom while keeping all the others in the system unchanged. Hence different configurations with the same number of negative bonds can belong to different classes.

Interestingly, 2D lattices with any nominal disorder can be also found in configurations of vanishing GI disorder. For example, if we start from a lattice with all bonds of positive sign, it is always possible to generate configurations with the required number of negative bonds by applying successive gauge transformations. However, the statistical weight of these configurations (among all configurations) is small and decreases with N. In other words, if we generate lattices with a nominal disorder p by choosing the sign of each bond randomly, there is a negligible chance to obtain a configuration with no GI disorder. On the contrary, in statistically-relevant configurations (thermodynamic limit), there is an irreducible fraction of negative bonds which, in average, is given by a certain function of p that we call $p_r(p)$.

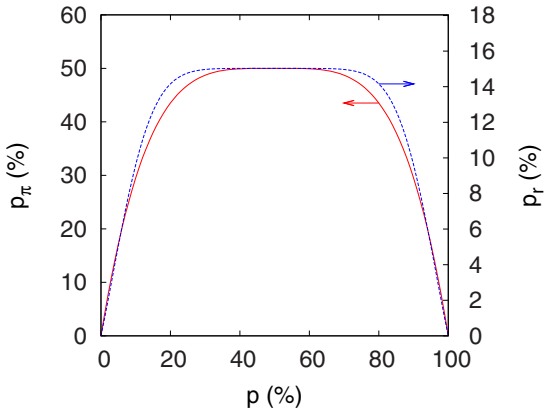

FIG. 3. Relative amount p_π of plaquettes with π flux (red solid curve) and p_r of GI disorder (blue dashed curve) versus nominal disorder p, for lattices with bond-sign disorder. The standard deviation induced by the calculations on sets of systems of finite size is below 10^{-3}% on p_π and 0.2% on p_r.

B. Analogy with spin glasses

The determination of the GI disorder in a general lattice with bond-sign disorder is a complex problem which, however, can be achieved following methodologies which were developed many years ago to study the physics of spin glasses [45,47]. If we consider a random Ising spin system with a variable concentration of mixed nearest-neighbor exchange couplings $\pm J$ on a square lattice (a well-known model of spin glass), the ground state of the system is characterized by an irreducible disorder, i.e., a frustration [45,46]. As explained in Ref. [25], the search for the ground state in this model and the determination of the GI disorder in lattices with bond-sign disorder are mathematically equivalent problems. Therefore we could use the algorithm developed in Ref. [53] to determine the GI disorder. In the present work, we preferred to employ the more recent and more efficient algorithm of Ref. [54]. Using the program based on this algorithm and available in the public domain [55], we have determined the GI disorder for a random set of lattices, for different values of the nominal disorder p, and we have deduced the amount of GI disorder $p_r(p)$. This function will be used for the interpretation of disorder effects on the electronic states.

The evolution of p_r with p, presented in Fig. 3, is consistent with previous calculations [46,53]. For small values of p, the GI and nominal disorders almost coincide [$p_r \approx p$]. In this regime of weak disorder, the negative bonds have a high probability to be isolated from each other. Thus it is not possible to reduce their number by applying gauge transformations without creating more negative bonds during the procedure. On the contrary, the saturation of p_r above ~25% takes place when, in average, there is more than one negative bond per site. In that case, the number of negative bonds can be efficiently reduced by successive gauge transformations.

C. Flux per plaquette

The bond-sign disorder that we are considering here could be seen as the effect of a spatially varying magnetic field carrying a 0 or π flux per plaquette of the square lattice. The flux is 0 (π) if the product of the bond signs along the edges of the plaquette is positive (negative). Since this flux is gauge-invariant [45,47], the map of the flux on a given sample provides a representation of its disorder configuration. If we are interested in statistically-relevant configurations (thermodynamic limit), the relative amount of plaquettes with π flux (hereafter, p_π) is another measure of the true disorder present in the system, in addition to p_r.

Figure 3 shows p_π calculated as a function of the nominal disorder p. Big lattices ($N = 5000$) were considered for the calculation in order to minimize statistical errors. The variations of p_π and p_r are clearly coherent. The highest value for p_π saturates at 50%. In samples of finite size, configurations with p_π between 50% and 100% exist but they are statistically unlikely. The (ordered) π-flux phase, which was extensively studied in different contexts cannot be seen as a clean limit of the bond-sign disorder problem.

For p close to 0% (or 100%), a linear relation between p_π and p_r is obtained ($p_\pi \approx 4p_r$). This was expected since negative bonds are isolated from each other and there are two plaquettes with π flux per negative bond (2 bonds per plaquette). However, at increasing nominal disorder, the coefficient of proportionality between p_π and p_r becomes smaller because the number of plaquettes with π flux tends to decrease when negative bonds get closer.

At the end of this section, it is interesting to come back to the definition of the nominal disorder p. Since p is not a gauge-invariant quantity, its setup requires to fix the local gauge. In the case of lattices of PbSe NCs, the sign of the hopping terms between neighbor NCs is determined by microscopic aspects. More generally, in artificial lattices, the sign can be controlled by their design and topology (see below, Sec. III G). As a consequence, these real systems are not exactly invariant by local gauge transformations, the bond-sign disorder is always accompanied by other types of disorder. However, in artificial lattices, their effects can be minimized as much as possible by careful design.

III. RESULTS AND DISCUSSION

In the following, we present results on the electronic structure of disordered lattices. These investigations are based on the full diagonalization of the Hamiltonian [Eq. (2)], for different values of N and p, for different configurations of the disorder (random choice of the bond sign).

A. DOS

The DOS averaged over 50 random configurations are presented in Fig. 4, for $p = 5$% and $p = 50$% ($N = 50$). The comparison with the DOS for the pristine square lattice shows that the bond-sign disorder has a significant effect on the electronic structure of 2D lattices, whereas it has no effect on 1D lattices. This confirms the existence in 2D of frustrations which do not exist in 1D. However, the bond-sign disorder has not the same influence on the electronic structure as other more conventional types of disorder. This can be seen by comparing with the DOS obtained for percolating lattices with 50% of broken bonds ($t = 0$) (Fig. 4). Note that this type of disorder is also present in lattices of PbSe NCs [42].

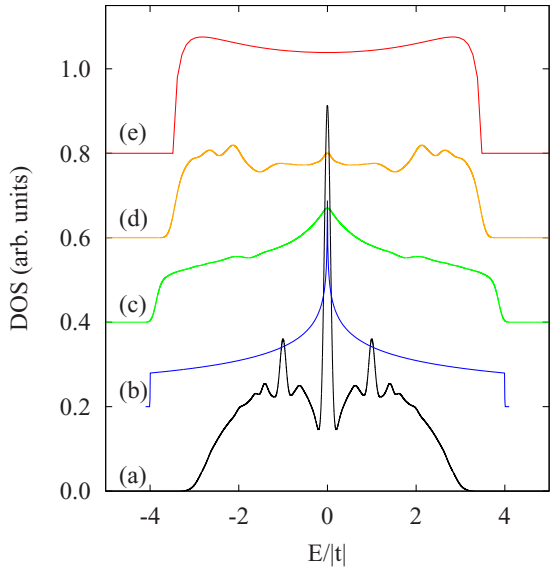

FIG. 4. DOS for different types of 2D square lattices. (a) Black line: percolating lattice with 50% of broken bonds (i.e., with $t = 0$). (b) Blue line: perfect lattice without disorder. (c) Green line: Lattice with a weak nominal bond-sign disorder ($p = 5\%$). (d) Orange line: lattice with the maximum nominal bond-sign disorder ($p = 50\%$). (e) Red line: infinite Bethe lattice. DOS for disordered lattices are calculated for $N = 50$ and are averaged over 50 configurations [standard deviation = 0.02 for (a), 0.003 for (c), and 0.01 for (d)].

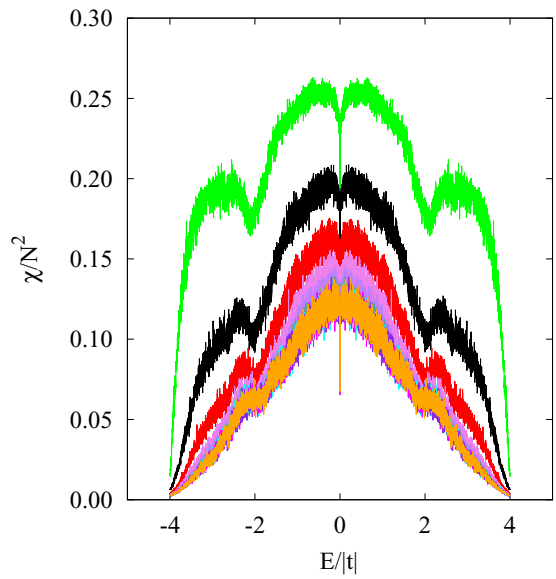

FIG. 5. Normalized participation ratio χ/N^2 for the electronic wave functions in 2D square lattices ($N = 100$) versus their energy, for different values of the nominal disorder: $p = 5\%$ (green), 10% (black), 15% (red), 20% (violet), 25% (purple), 30% (cadet blue), 35% (cyan), 40% (magenta), and 50% (orange) (standard deviation ≈0.04 for all curves).

B. Participation ratio

A convenient probe of the localization of the wave functions is the participation ratio χ defined for each state as $\chi = (\sum_i |c_i|^4)^{-1}$, where c_i is the complex amplitude of the wave function on the site i. χ measures the number of sites which contribute to the state. For its calculation, we have added to H a small on-site disorder (Gaussian distribution, standard deviation of $10^{-4}|t|$) in order to remove possible degeneracies of the eigenstates. This numerical treatment has a marginal effect on the values of χ, except at $E \approx 0$ for reasons which will be discussed in Sec. III E.

The results for 2D square lattices, averaged over the 100 random configurations, are depicted in Fig. 5 for different values of p. For the sake of comparison, χ is normalized by the total number (N^2) of sites in the sample since $\chi/N^2 = 1$ in absence of disorder.

Figure 5 shows that even a small amount of bond-sign disorder (e.g., 10%) induces a visible localization of the wave functions, not only near the band edges but also everywhere else in the energy spectrum. The localization increases with p but saturates above ∼25%. Remarkably, the real disorder experienced by the electrons is approximately the same between $p \approx 30\%$ and $p = 50\%$.

C. Correlation with the GI disorder

1. Localization vs GI disorder

The influence of the bond-sign disorder on the wave function localization is clearly visualized in Fig. 6(a), which displays $\overline{\chi/N^2}$ versus p, the overline representing the average over all energy states of the spectra. At increasing p, starting from 0, $\overline{\chi/N^2}$ first decreases, second starts saturating, and third becomes approximately constant for p above ∼25%. This behavior is directly related to the amount of GI disorder in the lattices. This is demonstrated by the clear correlation between the variations of $\overline{\chi/N^2}$ [Fig. 6(a)], p_r [Fig. 6(b)] and p_π (Fig. 3) with p. The saturation for p above ∼25% is a specific feature of the bond-sign disorder. In the case of more conventional forms of disorders, $\overline{\chi/N^2}$ usually tends to zero when the disorder is increased, as shown in Fig. 6(a) for the percolating lattice in which p represents the percentage of broken bonds. In that case, in the thermodynamic limit ($N \to \infty$), $\overline{\chi/N^2} \to 0$ for any value of p above 0.5, which corresponds to the bond percolation threshold for the square lattice.

2. DOS versus GI disorder

The influence of the disorder is also visible on the DOS (Fig. 4). In order to be more quantitative, it is instructive to calculate the moments of the DOS. These quantities are also very useful for the description of disordered systems [56,57]. The p^{th} moment of a DOS $n(E)$ is defined as

$$\mu_p = \int_{-\infty}^{\infty} E^p n(E) dE. \tag{3}$$

In the present case, all moments of odd order vanish due to the symmetrical character of the DOS. In Appendix B, we show that μ_2 is independent of the amount of disorder. As a consequence, μ_4 is the first moment that characterizes the real effect of the disorder on the DOS and we provide its analytic expression in Appendix B. Figure 6(b) displays the variations of the normalized moment $\mu_4/\mu_4(0)$ as a function of p, $\mu_4(0)$ being the moment in absence of disorder. Starting from $p = 0$, the normalized moment is a decreasing function of p but

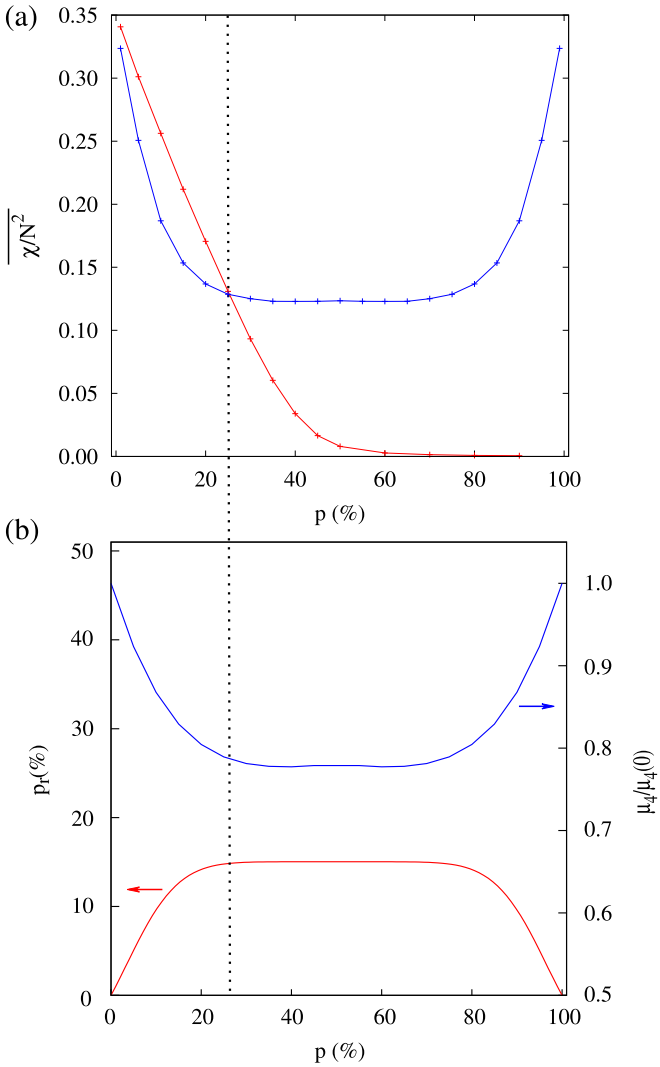

FIG. 6. (a) Average normalized participation ratio $\overline{\chi/N^2}$ vs p for lattices with bond-sign disorder (+, blue curve) and for percolating lattices (×, red curve). (b) Amount of GI disorder p_r (red curve) and normalized fourth moment of the DOS $\mu_4/\mu_4(0)$ vs p, for lattices with bond-sign disorder. The curve for p_r is the same as in Fig. 3 and is reproduced here for the sake of comparison.

reaches a saturation regime for $p \gtrsim 25\%$. Once again, this behavior is explained by the evolution of p_r with p [Fig. 6(b)], the modifications of the DOS are correlated with the amount of GI disorder.

The ratio μ_4/μ_2^2 is known to be a measure of the bimodal character of the DOS. As shown in Fig. 4, this bimodal character becomes pronounced when the bond-sign disorder is strong, which is consistent with a decrease of μ_4 with p (the second moment μ_2 being constant). In Appendix B, we discuss the physical origin of this behavior. We also explain why the DOS in the limit of strong disorder shares many similarities with the DOS calculated for the Bethe lattice (Fig. 4).

D. Localization length

In this section, we go deeper into the analysis of the wave function localization induced by the bond-sign disorder.

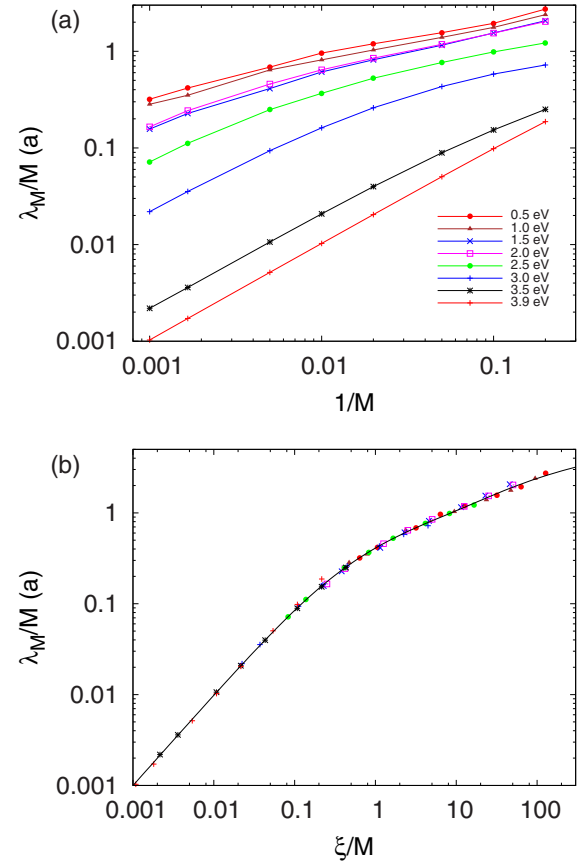

FIG. 7. Localization length λ_M for quasi-1D ribbons of width M in presence of a nominal bond-sign disorder p of 50%. (a) λ_M/M vs $1/M$, for different values of the normalized electron energy ($0.5 \leqslant |E/t| \leqslant 3.9$). (b) Scaling curve obtained from these data. The solid line is a fit with the scaling function $f(x) = d\ln(1 + x/d + bx^2 + cx^3)$ and $d = 0.24910$, $b = 0.15546$, and $c = 0.01279$.

We consider samples of quasi-1D geometry, of infinite length along the x direction. In the perpendicular direction y, the ribbon has a finite width of M sites. Figure 7 presents localization lengths calculated for maximum disorder ($p = 50\%$). The localization length λ_M is deduced from the calculation of the Lyapunov exponents using a transfer matrix formalism [58,59] as described in Appendix C. The plot of λ_M/M versus $1/M$ [Fig. 7(a)] clearly shows that the states for $|E/t| \geqslant 0.5$ are localized ($\lambda_M/M \to 0$).

The localization properties of the 2D system are then deduced from those of quasi-1D ones using scaling theory [59]. Figure 7(b) shows that the localization lengths of 1D ribbons satisfy a one-parameter scaling $\lambda_M/M = f(\xi/M)$, where ξa is the 2D localization length presented as function of the energy E in Fig. 8.

The 2D localization length tends to increases when one moves towards the center of the band. In that case, high values are found, exceeding 100 in units of the lattice spacing a for $|E| \lesssim 2.1$. This shows that the localization induced by the bond-sign disorder is not too strong, even for $p = 50\%$. However, it is interesting to see that localization lengths for bond-sign disorder are significantly smaller than in the random-flux model [34]. This means that random fluxes

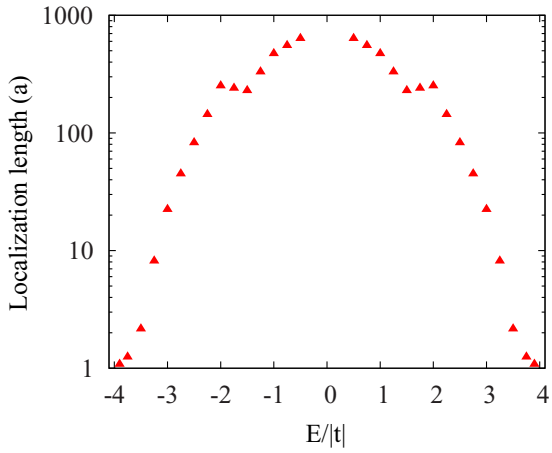

FIG. 8. 2D localization length versus normalized carrier energy $E/|t|$ for the 2D system.

scatter the electrons more efficiently in the $\{0, \pi\}$ ensemble than in $[-\pi, \pi]$.

It is interesting to compare the localization length (Fig. 8) with the participation ratio χ (Fig. 5), which was presented in Sec. III B. As can be seen, the two quantities seem to track each other, they exhibit similar behavior. This comparison cannot be more quantitative since χ was calculated for a system size smaller than (or comparable to) the localization length, i.e., χ is not converged. However, this suggests a regular behavior of the participation ratio with respect to the localization length, whereas a singular behavior was found in the Anderson model with strong bounded diagonal disorder [60].

E. Critical behavior at zero energy

The case of the band center ($E = 0$) requires specific attention. Figure 9 shows that λ_M/M remains approximately constant when the width M of the ribbon is increased, which tends to indicate that the zero-energy state is not localized. In addition, the value of the localization length depends on the parity of M. It is important to note that the results of Fig. 9 have been obtained assuming periodic conditions at the boundaries of the ribbons (in the y direction). If we use free boundary conditions, the calculation of λ_M/M diverges for odd M.

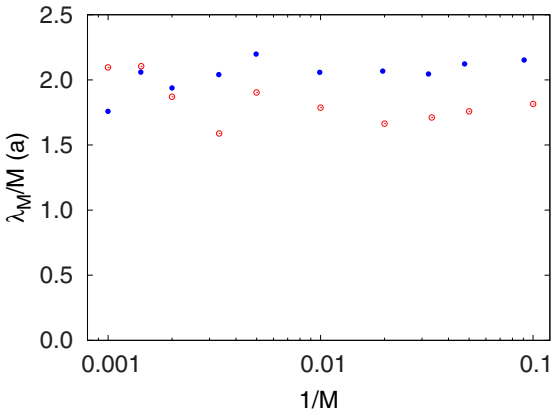

FIG. 9. Same as in Fig. 7(a) but for $E = 0$. λ_M/M is shown as function of $1/M$ for even (red circles) or odd (blue dots) values of the quasi-1D ribbons of width M.

Remarkably, very similar behaviors (delocalization of the states near the band center, influence of parity and boundary conditions) have been found with the random-flux model, i.e., for square lattices in which a static magnetic field is randomly distributed with zero mean [27–31,33,34,36]. The existence of extended states was also found in the model proposed by Gade [26], as well as in 1D [4,5] and 2D [6–8] systems with off-diagonal (random hopping) disorder, including in presence of π flux [32,35]. All of these systems have their own characteristics but they are all characterized by a sublattice (chiral) symmetry implying that, for every state of energy E, there is a state with energy $-E$ [31,61]. In this context, states at $E = 0$ are special since they may transform into themselves under the chiral symmetry operation. This implies in many cases diverging DOS and localization length near the band center [26]. At zero temperature, the extended systems are metallic at $E = 0$ but insulating at any other energy, $E = 0$ is a critical point.

Chiral and particle-hole symmetries, which hold for each configuration of disorder on the hopping terms, are thus verified in presence of bond-sign disorder. Combined with the results of Fig. 9, this supports a critical character of the zero-energy point but deeper theoretical studies are certainly necessary to confirm. In addition, it would be interesting to see whether the DOS diverges at $E = 0$, like in Gade [26] and random-flux [34] models for example. The present calculations (Fig. 4) do not allow to conclude as the singularity in the DOS may be extremely sharp.

It is important to mention that the delocalization at the band center is destroyed by on-site disorder which breaks the particle-hole symmetry [32,34]. Therefore the calculations of the participation ratio which were presented in Sec. III B and which include small on-site disorder terms (Fig. 5) cannot be used to investigate the wave function properties at $E = 0$.

F. The case of lattices of PbSe NCs

We now consider the square lattices of PbSe NCs studied experimentally and theoretically in Ref. [42]. The measured disorder is described in the calculations of the electronic structure by including fluctuations of the on-site and hopping energies and by taking into account the fraction (∼20%) of missing bonds between neighbor NCs. In these conditions, it is found that the localization length is smaller than $6a$. Even if the fraction of missing bonds was reduced to 5%, the localization length would remain smaller than $20a$. In these calculations, the bond-sign disorder was not considered. However, by comparison with the results of the previous section, we can conclude that the bond-sign disorder would not contribute to limit the localization length in a significant way. Therefore its neglect in Ref. [42] is justified by the present work.

G. Bond-sign disorder in artificial lattices

In lattices of PbX NCs, the bond-sign disorder cannot be present alone because it comes from the NC size dispersion

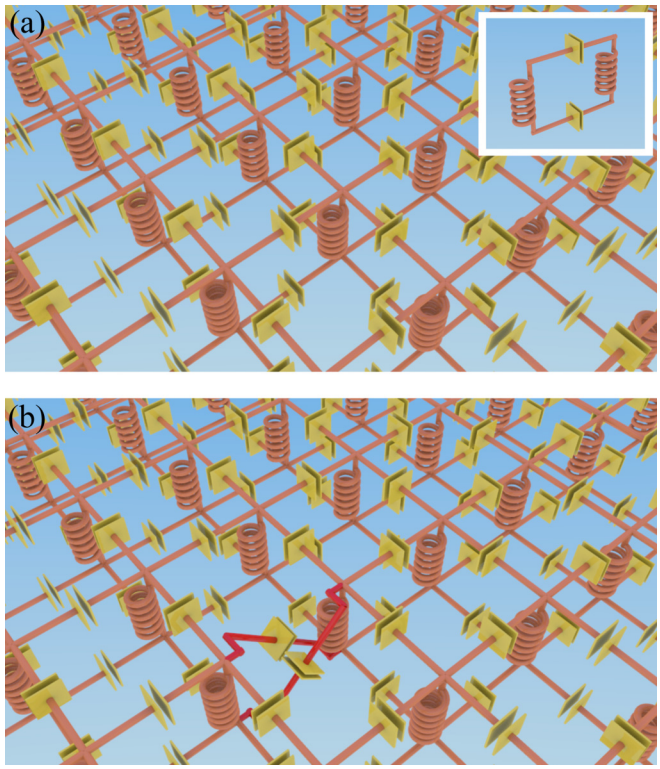

FIG. 10. (a) RF circuit consisting of a square lattice of coupled inductances. Inductances play the role of sites and capacitances the role of bonds. The inset shows the simple case of two connected sites. (b) A bond-sign can be changed by inverting the connections between the nodes of two first-nearest-neighbor inductances (red connections).

which is also at the origin of fluctuations of the on-site and hopping energies. Thus its experimental investigation would be much easier in dedicated artificial lattices in which other types of disorder could be minimized.

A way of implementing the bond-sign disordered lattices can be found in the realm of Radio-Frequency (RF) circuits. Indeed, it was shown using Bloch theory [62] that the dispersion relations of 2D negative-refractive-index transmission lines can be intuitively explained by the concepts of band structures in 2D Brillouin zones. The structure consists of LC resonators coupled through capacitances. In certain cases, it is possible to neglect the capacitance of the resonator. This approximation leads to a simpler version of these systems where each inductance plays the role of a site [Fig. 10(a)] [63]. Interestingly, it is possible to invert the sign of the coupling simply by inverting the connections between the nodes of two first nearest-neighbor inductances [Fig. 10(b)]. A single inversion of this type is irreducible and acts as a frustration within the lattice. On the contrary, a site with four negative bonds is reducible to zero negative bond just by a vertical flip of the inductance. This action is equivalent to a local gauge transformation discussed in previous sections. Interestingly, a more complex braiding of connections was recently used to create topologically nontrivial phases in such LC circuits [63].

IV. CONCLUSION

We have shown that the bond-sign disorder induces localization of the electronic wave functions in 2D square lattices, except at the band center. The true disorder seen by the electrons is an irreducible part of the nominal disorder specified by the relative fraction of bonds with a negative hopping term. The electronic properties, including the DOS and the localization length, are only sensitive to this irreducible disorder, which results from frustrations that cannot be removed by local gauge transformations. This work was originally motivated by studies on lattices of PbSe NCs in which the size dispersion leads to bond-sign disorder, in addition to more conventional types of disorder. However, our results show that the effects of the bond-sign disorder in these systems are not the dominant ones.

Another interesting feature of the bond-sign disorder is the critical character of the zero-energy point characterized by a diverging localization length. This type of behavior is already well-known as it was found in disordered 2D lattices in which there is a sublattice (chiral) symmetry [26–36]. The present work is quite general, it should motivate further experimental studies on artificial lattices in which we could generate bond-sign disorder on demand.

ACKNOWLEDGMENT

This work was supported by the French National Research Agency (Dirac-III-V project ANR-16-CE24-0007-01).

APPENDIX A: ATOMISTIC TIGHT-BINDING CALCULATIONS OF THE BAND STRUCTURE OF PBSE NC LATTICES

The band structure of square lattices of PbSe NCs shown in Fig. 2 was calculated using the atomistic tight-binding method. Each atom in the lattice (Pb or Se) is described by a double set of $sp^3d^5s^*$ atomic orbitals including the spin degree of freedom [44]. Spin-orbit coupling is included.

We have considered 2D lattices of $\langle 001\rangle$-oriented NCs attached via perpendicular {100} facets. Each NC has the form of a truncated nanocube, comprising six {100}, eight {111}, and twelve {110} facets. The positions of the vertices of the NC shape are given by $P[\pm 1, \pm(1-q), \pm(1-q)]$, where $[\pm 1, \pm 1, \pm 1]$ indicate the position of the six corners of the original nanocube ($q = 0$), q is the truncation factor and P represents all possible permutations. The results presented in this paper have been obtained for $q = 0.45$. The length of the vectors delineating the superlattice is na_0 where n is an integer and a_0 is the lattice parameter (0.612 nm for PbSe). Details on the calculation methodology can be found in Ref. [40].

APPENDIX B: MOMENTS OF THE DOS

The moment of order p [Eq. (3)] can be rewritten as

$$\mu_p = \frac{1}{N^2}\,\mathrm{Tr}\,H^p = \frac{1}{N^2}\sum_{\alpha}\langle\alpha|H^p|\alpha\rangle \qquad \text{(B1)}$$

where the sum is over the orbitals $|\alpha\rangle$ on the $N \times N$ sites of the system and H is the Hamiltonian. The moment can be

expressed under the form

$$\mu_p = \frac{1}{N^2}\sum_{\alpha}\left[\sum_{\alpha_1\cdots\alpha_{p-1}} \langle\alpha|H|\alpha_1\rangle\langle\alpha_1|H|\alpha_2\rangle\cdots\langle\alpha_{p-1}|H|\alpha\rangle\right]. \tag{B2}$$

The calculation of the term in the bracket of Eq. (B2) requires to consider all possible different circuits of p walks authorized by the Hamiltonian matrix elements, starting and ending on the orbital $|\alpha\rangle$. μ_p is given by the average of these terms over all the orbitals. In a pristine square lattice, these terms are all identical. Therefore, in presence of disorder, μ_p is given by the statistical average of the bracketed term over the different configurations of disorder.

In the specific case of the bond-sign disorder, the second-order moment is not altered because it only includes terms of the form $|\langle\alpha|H|\alpha_1\rangle|^2$ in which the sign of the matrix element is unimportant. For the square lattice, since each site has four nearest neighbor, μ_2 is equal to $4|t|^2$.

The fourth-order moment μ_4 is thus the first nonzero moment, which depends on the disorder. In order to calculate it, we have considered all possible circuits of 4 walks, which are 36 in number. Each circuit contributes to the moment as a term $|t|^4$ multiplied by the product of the sign of each bond on the circuit. Taking into account the probability p to have a negative bond, we obtain after some algebra

$$\mu_4 = 28|t|^4 + 8|t|^4(2p-1)^4. \tag{B3}$$

We have checked that Eq. (B3) fits perfectly with the numerical results of Fig. 6(b). For $p = 0$, μ_4 is maximum $(36|t|^4)$ because the terms associated with the 36 circuits all come with a positive sign. For $p \neq 0$, there are 28 circuits in which each hop between two neighbor sites is done back and forth. The corresponding 28 terms thus remain unaltered because all signs are squared. Only eight circuits in the form of squares (of side a) give terms influenced by the bond-sign disorder. For $p = 50\%$, their contributions cancel out since there is the same probability to find them with a positive or negative sign ($\mu_4 = 28|t|^4$). This explains why μ_4 decreases in presence of disorder [Fig. 6(b)].

It is interesting to compare the present results with those obtained for the same Hamiltonian but on a Bethe lattice in which each node is connected to four neighbors [64]. By construction, a Bethe lattice is cycle-free and therefore μ_4 is equal to $28|t|^4$, like for the square lattice with $p = 50\%$. As a consequence, it can be anticipated that the two systems have comparable DOS. This is indeed confirmed in Fig. 4, which shows that the DOS for the square lattice increasingly resembles the DOS for the Bethe lattice [65] when the amount of bond-sign disorder is increased. In particular, the bimodal character of the DOS becomes more pronounced.

APPENDIX C: CALCULATION OF THE LYAPUNOV EXPONENTS

We consider a ribbon of M atoms in width, with free boundary conditions except otherwise stated. The 1D lattice is divided into successive strips. The wave function in the strip n is denoted $|\Psi_n\rangle$. The Schrödinger equation at a given energy E is written as

$$H_{n,n}|\Psi_n\rangle + H_{n,n-1}|\Psi_{n-1}\rangle + H_{n,n+1}|\Psi_{n+1}\rangle = E|\Psi_n\rangle, \tag{C1}$$

where $H_{n,m}$ is the Hamiltonian matrix between strips n and m. Equation (C1) can be rewritten in a matrix form as

$$\begin{pmatrix}|\Psi_{n+1}\rangle\\ |\Psi_n\rangle\end{pmatrix} = T_n\begin{pmatrix}|\Psi_n\rangle\\ |\Psi_{n-1}\rangle\end{pmatrix}, \tag{C2}$$

where T_n is a transfer matrix

$$T_n = \begin{pmatrix}H_{n,n+1}^{-1}[E - H_{n,n}] & -H_{n,n+1}^{-1}H_{n,n-1}\\ 1 & 0\end{pmatrix}. \tag{C3}$$

Thus, given initial values $|\Psi_0\rangle$ and $|\Psi_1\rangle$, the wave function for any strip can be obtained by iteration,

$$\begin{pmatrix}|\Psi_{n+1}\rangle\\ |\Psi_n\rangle\end{pmatrix} = M_n\begin{pmatrix}|\Psi_1\rangle\\ |\Psi_0\rangle\end{pmatrix}, \tag{C4}$$

where $M_n = T_1T_2\cdots T_{n-1}T_n$.

The Lyapunov exponents are calculated as follows [58,66]. We consider $2M$ (dimension of T_n) normalized vectors $\mathbf{v}_i$. We multiply each vector successively by L transfer matrices chosen from a random sequence and we orthogonalize them using Gram-Schmidt algorithm. We calculate the norm d_k^i of the vectors and we normalize them. The procedure is repeated N times ($k = 1\cdots N$). The Lyapunov exponents γ_i ($i = 1\cdots 2M$) are then given by

$$\gamma_i = \frac{1}{NL}\sum_{k=1}^{N}\ln\left(d_k^i\right). \tag{C5}$$

In the present work, we used $N = 10^4$ and $L = 10$, which ensures good convergence and numerical accuracy of the results. The localization length λ_M is defined as the bond length a divided by the smallest positive Lyapunov exponents.

[1] P. W. Anderson, Phys. Rev. **109**, 1492 (1958).
[2] E. Abrahams, P. W. Anderson, D. C. Licciardello, and T. V. Ramakrishnan, Phys. Rev. Lett. **42**, 673 (1979).
[3] P. A. Lee and T. V. Ramakrishnan, Rev. Mod. Phys. **57**, 287 (1985).
[4] H. Hermann and J. Schreiber, Phys. Status Solidi B **67**, K93 (1975).
[5] G. Theodorou and M. H. Cohen, Phys. Rev. B **13**, 4597 (1976).
[6] E. Economou and P. Antoniou, Solid State Commun. **21**, 285 (1977).
[7] T. P. Eggarter and R. Riedinger, Phys. Rev. B **18**, 569 (1978).
[8] A. Eilmes, R. Römer, and M. Schreiber, Eur. Phys. J. B **1**, 29 (1998).
[9] S. Kirkpatrick, Rev. Mod. Phys. **45**, 574 (1973).
[10] T. Odagaki, M. Lax, and A. Puri, Phys. Rev. B **28**, 2755 (1983).
[11] Y. Meir, A. Aharony, and A. B. Harris, EPL **10**, 275 (1989).
[12] D. S. Wiersma, P. Bartolini, A. Lagendijk, and R. Righini, Nature (London) **390**, 671 (1997).
[13] T. Schwartz, G. Bartal, S. Fishman, and M. Segev, Nature (London) **446**, 52 (2007).

[14] S. Karbasi, C. R. Mirr, P. G. Yarandi, R. J. Frazier, K. W. Koch, and A. Mafi, Opt. Lett. **37**, 2304 (2012).

[15] I. S. Graham, L. Piché, and M. Grant, Phys. Rev. Lett. **64**, 3135 (1990).

[16] H. Hu, A. Strybulevych, J. H. Page, S. E. Skipetrov, and B. A. van Tiggelen, Nat. Phys. **4**, 945 (2008).

[17] J. Billy, V. Josse, Z. Zuo, A. Bernard, B. Hambrecht, P. Lugan, D. Clément, L. Sanchez-Palencia, P. Bouyer, and A. Aspect, Nature (London) **453**, 891 (2008).

[18] G. Roati, C. D'Errico, L. Fallani, M. Fattori, C. Fort, M. Zaccanti, G. Modugno, M. Modugno, and M. Inguscio, Nature (London) **453**, 895 (2008).

[19] R. E. Chandler, A. J. Houtepen, J. Nelson, and D. Vanmaekelbergh, Phys. Rev. B **75**, 085325 (2007).

[20] P. Guyot-Sionnest, J. Phys. Chem. Lett. **3**, 1169 (2012).

[21] I. Carbone, S. A. Carter, and G. T. Zimanyi, J. Appl. Phys. **114**, 193709 (2013).

[22] J. Yang and F. W. Wise, J. Phys. Chem. C **119**, 3338 (2015).

[23] T. Chen, K. V. Reich, N. J. Kramer, H. Fu, U. R. Kortshagen, and B. I. Shklovskii, Nat. Mater. **15**, 299 EP (2015).

[24] L. Qu, M. Vörös, and G. T. Zimanyi, Sci. Rep. **7**, 7071 (2017).

[25] M. Schwalm and W. Schwalm, Int. J. Mod. Phys. B **15**, 3287 (2001).

[26] R. Gade, Nucl. Phys. B **398**, 499 (1993).

[27] Y. Avishai, Y. Hatsugai, and M. Kohmoto, Phys. Rev. B **47**, 9561 (1993).

[28] V. Kalmeyer, D. Wei, D. P. Arovas, and S. Zhang, Phys. Rev. B **48**, 11095 (1993).

[29] D. Z. Liu, X. C. Xie, S. Das Sarma, and S. C. Zhang, Phys. Rev. B **52**, 5858 (1995).

[30] D. N. Sheng and Z. Y. Weng, Phys. Rev. Lett. **75**, 2388 (1995).

[31] J. Miller and J. Wang, Phys. Rev. Lett. **76**, 1461 (1996).

[32] Y. Hatsugai, X.-G. Wen, and M. Kohmoto, Phys. Rev. B **56**, 1061 (1997).

[33] X. C. Xie, X. R. Wang, and D. Z. Liu, Phys. Rev. Lett. **80**, 3563 (1998).

[34] A. Furusaki, Phys. Rev. Lett. **82**, 604 (1999).

[35] T. Fukui, Nucl. Phys. B **562**, 477 (1999).

[36] V. Z. Cerovski, Phys. Rev. B **64**, 161101 (2001).

[37] W. H. Evers, B. Goris, S. Bals, M. Casavola, J. de Graaf, R. v. Roij, M. Dijkstra, and D. Vanmaekelbergh, Nano Lett. **13**, 2317 (2013).

[38] W. J. Baumgardner, K. Whitham, and T. Hanrath, Nano Lett. **13**, 3225 (2013).

[39] M. P. Boneschanscher, W. H. Evers, J. J. Geuchies, T. Altantzis, B. Goris, F. T. Rabouw, S. A. P. van Rossum, H. S. J. van der Zant, L. D. A. Siebbeles, G. Van Tendeloo, I. Swart, J. Hilhorst, A. V. Petukhov, S. Bals, and D. Vanmaekelbergh, Science **344**, 1377 (2014).

[40] E. Kalesaki, W. H. Evers, G. Allan, D. Vanmaekelbergh, and C. Delerue, Phys. Rev. B **88**, 115431 (2013).

[41] C. Delerue, Phys. Chem. Chem. Phys. **16**, 25734 (2014).

[42] K. Whitham, J. Yang, B. H. Savitzky, L. F. Kourkoutis, F. Wise, and T. Hanrath, Nat. Mater. **15**, 557 (2016).

[43] G. Bastard, *Wave Mechanics Applied to Semiconductor Heterostructures*, Monographies de Physique (Les Éditions de Physique, Les Ulis, 1988).

[44] G. Allan and C. Delerue, Phys. Rev. B **70**, 245321 (2004).

[45] G. Toulouse, Commun. Phys. **2**, 115 (1977).

[46] S. Kirkpatrick, Phys. Rev. B **16**, 4630 (1977).

[47] E. Fradkin, B. A. Huberman, and S. H. Shenker, Phys. Rev. B **18**, 4789 (1978).

[48] T. Weichao, Chin. Phys. Lett. **6**, 31 (1989).

[49] The situations for $p < 50\%$ and $p > 50\%$ are symmetric.

[50] T. Jacqmin, I. Carusotto, I. Sagnes, M. Abbarchi, D. D. Solnyshkov, G. Malpuech, E. Galopin, A. Lemaître, J. Bloch, and A. Amo, Phys. Rev. Lett. **112**, 116402 (2014).

[51] L. Lu, J. D. Joannopoulos, and M. Soljačić, Nat. Photon. **8**, 821 (2014).

[52] C. He, X. Ni, H. Ge, X.-C. Sun, Y.-B. Chen, M.-H. Lu, X.-P. Liu, and Y.-F. Chen, Nat. Phys. **12**, 1124 (2016).

[53] L. Bieche, J. P. Uhry, R. Maynard, and R. Rammal, J. Phys. A **13**, 2553 (1980).

[54] G. Pardella and F. Liers, Phys. Rev. E **78**, 056705 (2008).

[55] The programs are available on the server http://cophy.informatik.uni-koeln.de/research.html.

[56] F. Cyrot-Lackmann, J. Phys. C **5**, 300 (1972).

[57] F. Ducastelle, J. Phys. (France) **35**, 983 (1974).

[58] G. Benettin, L. Galgani, A. Giorgilli, and J.-M. Strelcyn, Meccanica **15**, 21 (1980).

[59] A. MacKinnon and B. Kramer, Z. Phys. B **53**, 1 (1983).

[60] S. Johri and R. N. Bhatt, Phys. Rev. Lett. **109**, 076402 (2012).

[61] P. Markoš and L. Schweitzer, Physica B: Condens. Matter **407**, 4016 (2012).

[62] A. Grbic and G. V. Eleftheriades, IEEE Trans. Antennas Propag. **51**, 2604 (2003).

[63] J. Ningyuan, C. Owens, A. Sommer, D. Schuster, and J. Simon, Phys. Rev. X **5**, 021031 (2015).

[64] H. A. Bethe, Proc. R. Soc. London A **150**, 552 (1935).

[65] E. Economou, *Green's Functions in Quantum Physics* (Springer, Berlin, 1979).

[66] J. Yang, Ph.D. thesis, Cornell University, 2015.